Static-Dynamics Decoupling in Responsive Matter Suspensions

Author: Berta Gómez Peinado
Facultat de Física, Universitat de Barcelona, Diagonal 645, 08028 Barcelona, Spain.

Advisor: José Manuel Ruiz Franco

Abstract: Responsive systems self-adapt their overall characteristics thanks to the presence of particles that modify their individual properties in response to external stimuli. Inspired by living matter and recent advances in material science, we perform numerical simulations to study slow dynamics suspensions in which particle elasticity can be tuned. In particular, we study the evolution of static and dynamic properties at two different elasticity states, observing that it is possible to speed up the particle dynamics without altering the overall static properties of the system.
Keywords: Responsive matter, slow dynamics, elasticity, Brownian particles.
SDGs: 4: Quality education, 9: Industry, innovation and infrastructure, 12: Responsible consumption and production and 17: Partnerships for the goals.

I. INTRODUCTION

Responsive matter refers to systems composed of particles that can modify their individual properties such as morphology and mechanical characteristics in response to external stimuli. This is the case for many living matters, which consist of agents whose motility and elastic properties can change depending on external factors such as chemical interactions, local agent concentration, or light [1, 2]. While significant effort has gone into understanding how external stimuli can modify motility in living systems [1], only recently has attention shifted toward studying changes in size and elasticity. To approach this scenario, recent advances in materials science and engineering have enabled the design particles with life-like properties that closely mimic the behavior of bioinspired materials with remarkable precision. For instance, synthetic hydrogel particles can exhibit periodic and synchronized oscillations in response to chemical feedback [3]. Additionally, computational models have been proposed to study the collective synchronization of size evolution in cells to capture the wave deformation emerging in living tissues [4].

In this work, we propose a simple model to study the impact of modifications in particle elasticity on the dynamic and static properties of highly concentrated particle systems. As a reference, we consider systems approaching dynamical arrest, such as supercooled liquids and glasses [5]. These systems are characterized to manifest slow dynamics as the volume fraction increases, a behavior governed by disordered structural configurations at the microscopic level. Indeed, the structural relaxation time τ_α, involving the complete relaxation of the system, increases at the characteristic length scale q in which the static structure factor $S(q)$ develops a peak. The increase of τ_α indicates that glasses, despite having the disordered structure typical of liquids, exhibit solid-like behavior. Similarly, diffusion may occur at longer timescales, or even be completely suppressed.

In order to summarize, in Section II we describe the numerical model and present the different quantities measured throughout the study to characterize both static and dynamic properties. In Section III, we discuss the results obtained, beginning with the approach to slow dynamics and continuing with the introduction of variations in particle elasticity. We conclude this section rationalizing how these variations affect the dynamical properties. Finally, in Section IV, we summarize the main findings and outline future modifications aimed at deepening our understanding of how specific particle activities can induce a decoupling between static and dynamic properties.

II. METHODS

A. Simulation details

We perform two-dimensional Molecular Dynamics simulations of a 50:50 binary mixture with $N = 10000$ Brownian particles of mass $m = 1$ and diameters $\sigma_A = 1.2$ and $\sigma_B = 0.8$, in order to avoid crystallization. Thus, these particles obey the equation of motion [6]

$$0 = \vec{F}^C + \vec{F}^D + \vec{F}^R \,, \tag{1}$$

where $\vec{F}^C = -\vec{\nabla} U_H\,(r)$ represents the conservative forces coming from the particle-particle interaction. Additionally, $\vec{F}^D = -\xi\vec{v}$ corresponds to the drag force, where ξ is the friction coefficient

$$\xi = \frac{k_B T}{D} \,, \tag{2}$$

where D is the translational diffusion coefficient. Finally, $\vec{F}^R$ captures the fluctuation force associated with the thermal noise called the random force. In particular, this random force is characterized by $\langle \vec{F}^R \rangle = 0$ and $\langle \vec{F}_i^R(t)\ \vec{F}_i^R(t') \rangle = 2\xi k_B T \delta(t-t')$ [6]. The equation of motion is solved using the Euler–Maruyama algorithm [6],

which is commonly employed to integrate stochastic differential equations, as described in Section A of the *Supplementary Material*.

The particle interaction, which defines the conservative forces, is described by a harmonic potential:

$$U_H = \epsilon_{ij}(r_c - r_{ij})^2 \; ; \quad r_{ij} < \sigma_{ij}, \tag{3}$$

with $\epsilon_{ij} = \sqrt{\epsilon_i \epsilon_j}$ being the particle elasticity, $\sigma_{ij} = 0.5\,(\sigma_i + \sigma_j)$ the particle diameter and r_{ij} the distance between two particles. In our simulations, length, mass, and energy are measured in units of $\langle\sigma\rangle$, m and ϵ, respectively. Thus, time is measured in units of $\tau = \sqrt{m\,\langle\sigma^2\rangle / k_B T}$. In the following, we will consider $k_B T$ and $D = 10\sigma^2/\tau$. Additionally, we vary the packing fraction ϕ, which determines the volume that occupies the particles of the system, and is defined as

$$\phi = \frac{N A_{\text{particles}}}{A} = \frac{\pi}{4}\,\langle\sigma^2\rangle\,\frac{N}{A}, \tag{4}$$

where $A = L^2$ is the area of the simulation box being L the box length. We apply periodic boundary conditions. All simulations are performed with LAMMPS [7].

B. Calculated observables

We analyze the static properties by computing the radial distribution function $g(r)$, which represents the probability of finding particles at a distance r. This function is related to the local density around a particle and is defined as [8]

$$g(r) = \frac{\langle\rho(r)\rangle}{\rho} = \frac{A}{N^2}\left\langle \sum_{i=1}\sum_{j\neq 1} \delta(\vec{r} - \vec{r}_{ij}) \right\rangle, \tag{5}$$

where $\vec{r}_{ij}$ is the distance between particle i and particle j and $\langle ... \rangle$ is the average over different configurations.

To obtain information about static correlations at long range, we compute the static structure factor $S(q)$, defined as [9]

$$S(q) = \frac{1}{N\,\overline{b^2(q)}}\left\langle \sum_{j,l} b_j(q) b_l(q) \exp\left(-i\vec{q}\cdot\vec{r}_{jl}\right) \right\rangle, \tag{6}$$

where $\vec{q} = \frac{2\pi}{L}\vec{m}$ (with $m \in \mathbb{Z}^2$) is the wavevector, $b_i(q)$ indicates the scattering amplitudes of one particle, and $\overline{b^2(q)}$ is for all particles. Adding $b_i(q)$ we are taking into account the polydispersity; in monodisperse systems, this variable would be $b_i(q) = 1$.

We also focus on the dynamic properties. In particular, we compute the mean squared displacement $\Delta r^2(t)$, which measures the average square distance made by a particle with respect to the initial position [8]:

$$\Delta r^2(t) = \left\langle \frac{1}{N}\sum_i \left[\vec{r}_i(t+\Delta t) - \vec{r}_i(t)\right]^2 \right\rangle, \tag{7}$$

where $\vec{r}_i$ represents the position of the i-th particle and Δt is the elapsed time.

Finally, we compute the collective intermediate scattering function $F_c(q,t)$ which relates the distance traveled by a particle relative to another particle in a Δt, providing information about density fluctuations [8]:

$$F_c\,(q^*, t) = \frac{1}{N}\left\langle \sum_{j,l}^{N} \exp\left[i\vec{q^*}\cdot\left(\vec{r}_j\,(t+\Delta t) - \vec{r}_l\,(t)\right)\right] \right\rangle, \tag{8}$$

at q^* vector corresponding to the length scale in which the $S(q)$ develops a main peak. This function allows us to study the dynamic correlations.

III. RESULTS

A. Approaching to slow dynamics

Our starting point is to bring the system close enough to the supercooled liquid state to observe characteristic slow dynamics. We approach a dynamical arrest state by increasing ϕ, and fixing the strength of interaction between all particles to be $\epsilon_{AA} = \epsilon_{BB} = 200 k_B T$. The resulting interaction is illustrated by the gray curve in Fig. 1(a).

We proceed as follows: we start at a low packing fraction, close to dilute conditions, with particles initially

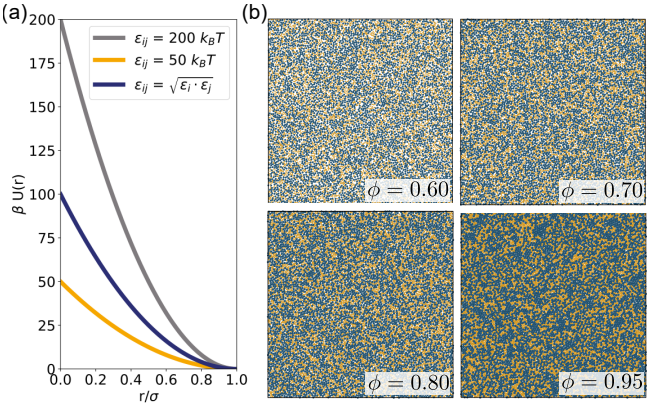

FIG. 1: **(a)** Harmonic potential interaction between particles for different elasticities. $\epsilon_{ij} = 200 k_B T$ is the elasticity among stiff particles whereas $\epsilon_{ij} = 50 k_B T$ is the elasticity among soft particles and $\epsilon_{ij} = \sqrt{\epsilon_i \epsilon_j}$ is the elasticity among stiff (ϵ_i) and soft particles (ϵ_j). **(b)** Snapshots depict the particles of simulation box with a different packing fractions ϕ. The colors indicate the particle type; small particles are yellow ($\sigma_B = 0.8$) and large particles are blue ($\sigma_A = 1.2$).

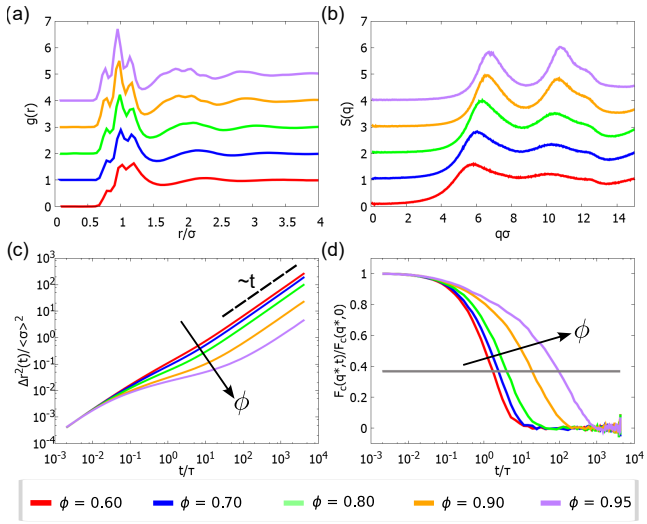

FIG. 2: Static and dynamic properties as a function of the packing fraction ϕ in equilibrium. **(a)** Radial distribution function $g(r)$. The data has been shifted up to improve visualization. **(b)** Static structure factor $S(q)$. The data has been shifted up to improve visualization. **(c)** Mean squared displacement $\Delta r^2(t)$. The discontinuous line highlights that the system diffuses at long times, and the arrow indicates where the packing fraction increases. **(d)** Intermediate scattering function $F_c(q^*, t)$. The arrow indicates where the packing fraction increases and the horizontal gray line represents $F_c(q^*, \tau_\alpha) = 1/e$.

placed at random positions. The system is then allowed to equilibrate, reaching a steady state where particles can explore the available space. After equilibration, we compute both the static and dynamic properties. To achieve higher packing fractions, we progressively compress the simulation box starting from the last equilibrated configuration to reach a desired new ϕ value. Snapshots of the system at different packing fractions are shown in Fig. 1(b). At each value of ϕ, we study the static and dynamic properties developed by the system.

In Fig. 2(a), we show the radial distribution function $g(r)$. At short length scales, we observe three peaks corresponding to the most probable distance between particles and their nearest neighbors. These peaks are the consequence of considering a binary mixture. Indeed, their positions are determined by their respective particle diameters, except for the middle peak which represents the average distance. This can be seen more clearly by computing the partial radial distribution functions $g_{\alpha\beta}$, shown in Section B of the *Supplementary Material*. Moving to larger distances, we see that the probability of finding particles beyond first neighbors tends to 1, resulting in the loss of correlation between particles.

Then, we compute the static structure factor $S(q)$, represented in Fig. 2(b), exhibiting two peaks. The presence of a first peak whose height increases with ϕ indicates the presence of static correlations at large scales. Surprisingly, a second prominent peak is also observed at intermediate $q-$values, indicating that a certain correlation is emerging at shorter distances. To gain insight, we also report the partial static structure factors $S_{\alpha\beta}$ for the largest (S_{AA}) and the smallest (S_{BB}) particles, shown in Section C of the *Supplementary Material*. While at low ϕ both functions develop a peak around $q = 2\pi/\sigma_i$, with $i \in [A, B]$, the second peak exhibited by $S(q)$ is related to static correlations coming from σ_A particles. Indeed, the snapshots in Fig. 1(b) reveals that increasing ϕ leads to the aggregation of same-sized particles, indicative of microphase separation.

Next, we focus on the dynamic properties. Fig. 2(c) shows the mean squared displacement $\Delta r^2(t)$. While for small ϕ values the dynamics is roughly diffusive throughout the entire time window, at higher packing fractions and in intermediate times, we can see a loss of the diffusive behavior because the dynamics becomes much slower. This slowdown arises from the increased frequency of particle collisions, which hinder the particle displacement and reduce diffusion, thereby lowering the overall dynamics. Thus, the system reaches a diffusive regime again at longer times (highlighted by the dashed line). Similarly, the collective intermediate scattering function $F_c(q^*, t)$ is computed at q^* value in which static correlations are observed. As shown in Fig. 2(d), $F_c(q^*, t)$ reveals slower dynamics with increasing ϕ, evidenced by the longer time required to reach decorrelation. This decay is associated with the α-mechanisms related to the system relaxation. We extract the corresponding structural relaxation time τ_α by imposing the condition $F_c(q^*, \tau_\alpha) = 1/e$. As reported in Section D of the *Supplementary material*, τ_α increases with ϕ, consistent with expectations when approaching a supercooled state [8].

Although a more detailed study would be required to accurately identify the dynamic transition from a liquid to a supercooled liquid, for our purposes, the system at $\phi = 0.95$ is sufficiently close to a dynamical arrest state. Therefore, in what follows, we focus on this packing fraction.

B. Responsive particle elasticity

Once the value of ϕ at which the system begins to exhibit slow dynamics has been identified, we investigate the evolution of the system when particle elasticity varies over time. In particular, we focus on the larger particles (diameter σ_A), and set their elasticity to switch between two fixed values: $\epsilon_{AA} = 200 k_B T$ and $\epsilon_{AA} = 50 k_B T$, as shown in Fig. 3(a). The gray and orange curves represented in Fig. 1(a) show the shape of the harmonic interaction when particles are stiffer and softer, respectively. In contrast, the elasticity of the smaller particles, i.e. those with diameter σ_B, remains fixed at $\epsilon_{BB} = 200 k_B T$. The blue curve in Fig. 1(a) illustrates the resulting interaction strength between particles of different elasticity when large particles are softer. We study scenar-

ios where we modify the fraction of larger particles n_A that can vary their elasticity. In particular, we focus on $n_A = 10\%, 20\%, 25\%, 50\%$ and 100%, and investigate the resulting changes in the static and dynamic properties, comparing them with one where elasticity is uniform, i.e. $n_A = 0\%$.

To illustrate the effects of elasticity changes in our system, we report two snapshots in Fig. 3 at different time intervals. The first snapshot, displayed in Fig. 3(b) shows particles with uniform elasticity, while Fig. 3(c) depicts a scenario where $n_A = 100\%$ becomes softer. Clear differences are evident between the two images. For situations where the elasticity is uniform, a more compact structure is observed. In contrast, when large particles are softer, they undergo significant deformation and the distance between particles decreases.

Then, we explore the effects of elastic changes on the static properties. In particular, we focus on $S(q)$ as a function of n_A, shown in Fig. 4(a). We observe that as n_A increases, the main peak slightly shifts toward large q. This shift indicates a decrease in the average interparticle distance, which we attribute to particle deformation. Nevertheless, the first peak remains stable across all simulations, exhibiting consistent height and position. Thus, we see that the structural correlation length at large scales does not depend on n_A. In contrast, the second peak progressively diminishes, indicating that the microphase separation is removed.

We now turn our attention to dynamic properties. Fig. 4(b) shows $\Delta r^2(t)$ as a function of n_A. A gradual presence of softer particles leads to faster dynamics. Indeed, the characteristic plateau developed at intermediate times begins to disappear. This observation indicates that softer particles can escape from microscopic regions at high local concentration, thereby enhancing the overall

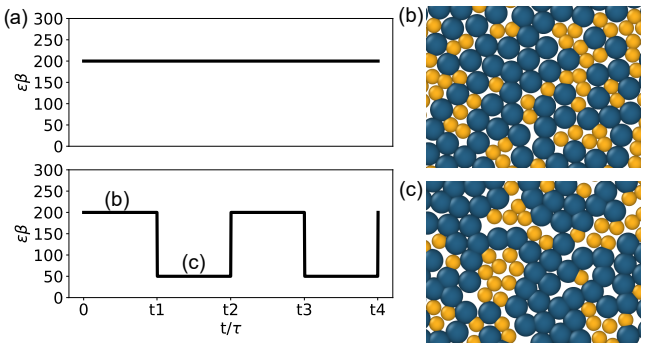

FIG. 3: **(a)** Elasticity as a function of time where the graph above represents the small particles (type B, yellow particles) and the graph below represent the large particles (type A, blue particles). **(b)** Zoom of a snapshot that depicts the configuration when particles have the same elasticity value ($\epsilon_{AA} = \epsilon_{BB} = 200 k_B T$). **(c)** Zoom of a snapshot that displays a configuration when all the larger particles become softer ($\epsilon_{AA} = 50 k_B T$, $\epsilon_{BB} = 200 k_B T$). The colors represent the particle size.

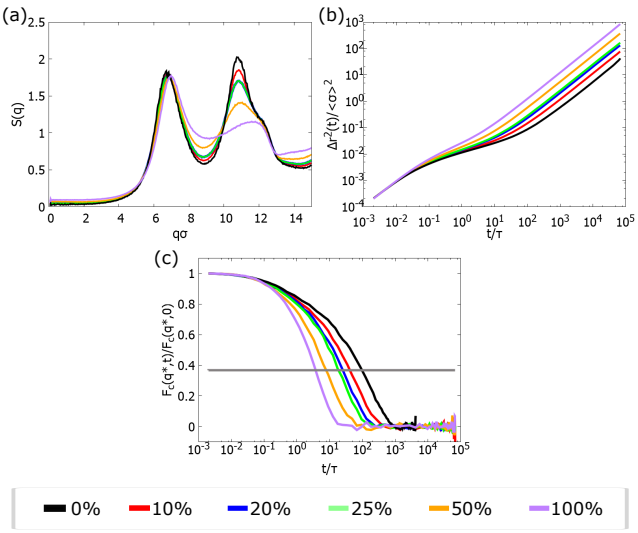

FIG. 4: Static and dynamic properties of the system as a function of the fraction of responsive particles n_A. The black line represents a simulation where the elasticity is uniform ($n_A = 0\%$). **(a)** Static structure factor $S(q)$. **(b)** Mean squared displacement $\Delta r^2(t)$. **(c)** Intermediate scattering function $F_c(q^*, t)$. The horizontal gray line represents $F_c(q^*, \tau_\alpha) = 1/e$.

system dynamics. This enhanced microscopic mobility is also consistent with the reduction observed in the second peak of $S(q)$. Furthermore, we compute $F_c(q^*, t)$, shown in Fig. 4(c). Similarly to the mean square displacement, larger n_A induces faster decay, as observed through the decrease in the relaxation time. As in the previous section, we extract τ_α reported in the Section D of the *Supplementary material*. We see that τ_α decreases as well as n_A increases. Therefore, we can see that by tuning the particle elasticity and the fraction of responsive particles, it is possible to accurately control the system dynamics while preserving static properties.

C. Impact on the dynamics

So far, we have shown that responsive particles enable us to modify dynamic properties while the static properties at large length scales remain unaffected. We therefore ask whether it is possible to rationalize these observations by establishing a mapping that compares the diffusion coefficient exhibited by the system at $n_A = 0\%$, defined as D_ϕ, with the diffusion coefficient that the system shows as a function of n_A, defined as D_n. We access the diffusion coefficient by considering that $\lim_{t\to\infty} \Delta r^2(t) = 4Dt$.

In Fig. 5(a), we represent D_ϕ as a function of ϕ (blue line, left axis) versus D_n as a function of n_A (green line, right axis). As previously discussed, an increase in ϕ leads to slower system dynamics, which is clearly captured by a decline in D_ϕ. In contrast, an increase in

n_A results in faster system dynamics, manifested by an enhancement in D_n. Then, to establish the mapping, we compare different systems that exhibit the same diffusion coefficients, i.e. $D_\phi = D_n$. This allows us to identify what systems with a specific dynamic behavior as a function of n_A correspond to systems with an effective packing fraction ϕ_{eff}. The mapping is shown in Fig. 5(b). As a result, varying n_A promotes that the system experiences lower ϕ_{eff} values, even though the overall geometric packing fraction of the system remains constant at $\phi = 0.95$, since the particle sizes are not modified (see Eq. 4 for the definition of packing fraction). Note that this mapping could be performed by considering the structural relaxation time, yielding to similar conclusions.

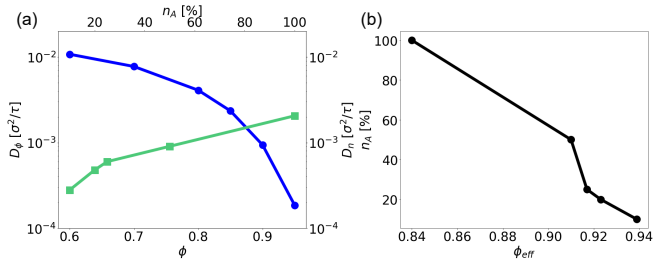

FIG. 5: **(a)** The diffusion coefficient D_ϕ as a function of the packing fraction ϕ (blue line) versus the diffusion coefficient D_n as a function of the fraction particles changing elasticity n_A (green line). **(b)** Mapping between n_A and the effective packing fraction ϕ_{eff}.

IV. CONCLUSIONS

In this work, we propose a simple model to study the effects that the particle elasticity has on the static and dynamic properties of a binary mixture. We have observed that systems with the same packing fraction ϕ can exhibit different dynamical behaviors, although their static properties related to long-range correlations remain unaffected. Note that restoring the uniform elasticity, we recover the characteristic slow dynamics for a system with $\phi = 0.95$, and hence, same static and dynamic properties. From the experimental point of view, this scenario could be reproduced using polymeric colloidal particles such as microgels [9]. These colloidal particles exhibit Brownian dynamics. Nevertheless, the internal polymer structure provides degrees of freedom to make them responsive to external stimuli such as temperature, pH or external fields [10].

In the future, we will extend this investigation by studying the dynamical properties of the system within time windows where multiple elastic changes are considered. This approach will offer a pathway to explore active matter, which refers to systems composed of particles that transform energy into work. This work typically results in motion and is observed across scales, from microscopic entities like cells and artificial microswimmers to macroscopic systems such as flocking birds or humans [11]. In our case, we plan to assume that active particles consume energy to modify their internal elasticity. Furthermore, it would be interesting to explore the effects of randomly varying the number of particles that change their elasticity over time.

Acknowledgments

I would like to thank for the constant guidance, help and dedication of my advisor, José Manuel Ruiz Franco, throughout the project. Thanks to him, I have been able to enter the world of research through simulations. I would also like to thank my family, friends and partner for all the support, with a special mention to my father, Miguel Ángel Gómez Gámiz.

[1] Frangipane, G. *et al.* Dynamic density shaping of photokinetic e. coli. *Elife* **7**, e36608 (2018).
[2] Gnan, N. & Maggi, C. Critical behavior of quorum-sensing active particles. *Soft Matter* **18**, 7654–7661 (2022).
[3] Blanc, B. *et al.* Collective chemomechanical oscillations in active hydrogels. *Proceedings of the National Academy of Sciences* **121**, e2313258121 (2024).
[4] Zhang, Y. & Fodor, É. Pulsating active matter. *Physical Review Letters* **131**, 238302 (2023).
[5] Janssen, L. M. Mode-coupling theory of the glass transition: A primer. *Frontiers in Physics* **6**, 97 (2018).
[6] Allen, M. P. & Tildesley, D. J. *Computer simulation of liquids* (Oxford university press, 2017).
[7] Plimpton, S. Fast parallel algorithms for short-range molecular dynamics. *Journal of computational physics* **117**, 1–19 (1995).
[8] Binder, K. & Kob, W. *Glassy materials and disordered solids: An introduction to their statistical mechanics* (World scientific, 2011).
[9] Ruiz-Franco, J. *et al.* Concentration and temperature dependent interactions and state diagram of dispersions of copolymer microgels. *Soft matter* **19**, 3614–3628 (2023).
[10] Scheffold, F. Pathways and challenges towards a complete characterization of microgels. *Nature communications* **11**, 4315 (2020).
[11] Toschi, F. & Sega, M. *Flowing matter* (Springer Nature, 2019).

Desacoblament estàtic-dinàmic en suspensions de matèria sensitiva

Author: Berta Gómez Peinado
Facultat de Física, Universitat de Barcelona, Diagonal 645, 08028 Barcelona, Spain.

Advisor: José Manuel Ruiz Franco

Resum: Els sistemes sensitius autoadapten les seves característiques generals gràcies a la presència de partícules que modifiquen les seves propietats individuals en resposta a estímuls externs. Inspirats en la matèria viva i els avenços recents en la ciència de materials, realitzem simulacions numèriques per estudiar suspensions de dinàmica lenta on es pot ajustar l'elasticitat de les partícules. En particular, estudiem l'evolució de les propietats estàtiques i dinàmiques en dos estats d'elasticitat diferents, observant que és possible accelerar la dinàmica de les partícules sense alterar les propietats estàtiques generals del sistema.
Paraules clau: Matèria sensitiva, dinàmica lenta, elasticitat, partícules Brownianes.
ODSs: Aquest TFG està relacionat amb els Objectius de Desenvolupament Sostenible (SDGs)

Objectius de Desenvolupament Sostenible (ODSs o SDGs)

1. Fi de la es desigualtats		10. Reducció de les desigualtats	
2. Fam zero		11. Ciutats i comunitats sostenibles	
3. Salut i benestar		12. Consum i producció responsables	X
4. Educació de qualitat	X	13. Acció climàtica	
5. Igualtat de gènere		14. Vida submarina	
6. Aigua neta i sanejament		15. Vida terrestre	
7. Energia neta i sostenible		16. Pau, justícia i institucions sòlides	
8. Treball digne i creixement econòmic		17. Aliança pels objectius	X
9. Indústria, innovació, infraestructures	X		

Aquest TFG està relacionat amb diferents ODS. La primera seria l'ODS 4, concretament la fita 4.7, ja que s'està cursant un grau universitari. També ho podem relacionar amb l'ODS 9, concretament les fites 9.5 i 9.7, i amb l'ODS 12, amb la fita 12.6, perquè una investigació sobre la matèria activa pot proporcionar coneixements per millorar nous materials o tecnologies sostenibles. Per últim, l'intercanvi de coneixement proporcionat per la bibliografia es podria relacionar amb l'ODS 17, amb les fites 17.16 i 17.17.

GRAPHICAL ABSTRACT (OPTIONAL)

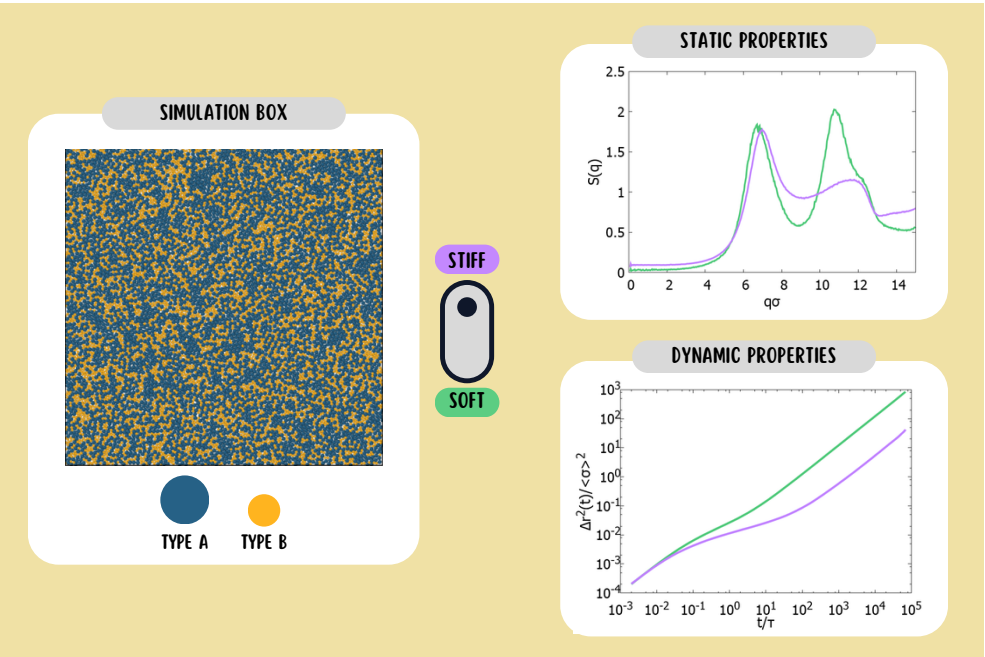

SUPPLEMENTARY MATERIAL (OPTIONAL)

A. Euler-Maruyama

In order to determine the displacement of the particles in our system, we need to solve our equation of motion (Eq. 1) explained in Section II. The method used to do this is the Euler-Maruyama algorithm. This method is obtained by using an enhanced Euler [6]

$$\vec{r}_i(t+\Delta t) = \vec{r}_i(t) + \vec{F}_i^C \ \Delta t + \vec{F}_i^R(t)\sqrt{\Delta t}. \tag{9}$$

where Δt is the timestep. This algorithm is typically used to study Brownian motion, which arises from Langevin dynamics in the overdamped limit, i.e. $\xi \to \infty$.

B. Partial radial distribution functions $g_{\alpha\beta}(r)$

In Fig. 6 we represent the partial radial distribution functions $g_{\alpha\beta}(r)$ as a function of the packing fraction ϕ, defined as [8]

$$g_{\alpha\beta}(r) = \frac{A}{N_\alpha N_\beta} \left\langle \sum_i^{N_\alpha} \sum_j^{N_\beta} \delta(\vec{r} - \vec{r}_{ij}) \right\rangle. \tag{10}$$

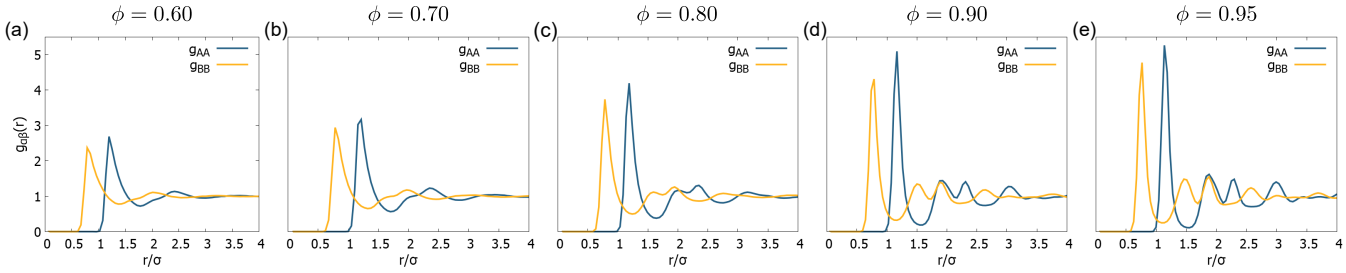

FIG. 6: Partial radial distribution function $g_{\alpha\beta}(r)$ for the two different types of particles at different packing fractions. The blue color represent the largest particles ($\sigma_A = 1.2$) and the yellow color represents the smallest particles ($\sigma_B = 0.8$).

We observe a main peak related to particles' size for each particle. The other oscillations at larger distances are different regarding to a liquid, due to our system being polydisperse with some particles' aggregation. These defects are observed in the total radial distribution function. Additionally, an increase in the intensity of the peaks is observed since as the distance between particles decreases (the packing fraction increases), the probability of finding particles increases.

C. Partial static structure factors $S_{\alpha\beta}(q)$

Fig. 7 shows the partial static structure factors $S_{\alpha\beta}(q)$ as a function of ϕ, defined as [8]

$$S_{\alpha\beta}(q) = \frac{1}{N_{\alpha\beta}\ \overline{b^2(q)}} \left\langle \sum_j^{N_\alpha} \sum_l^{N_\beta} b_j(q) b_l(q) \exp\left(-i\vec{q}\cdot\vec{r}_{jl}\right) \right\rangle. \tag{11}$$

We observe a double contribution for the largest particles and a simple contribution for smallest ones. At $q \to 0$ there is some noise which may be due to particles' agglomerations. This group of particles can lead to small-scale phase separation, as observed in two-dimensional experiments. Moreover, the main peak shifts at larger q by increasing ϕ, highlighting that the particles are more closely packed.

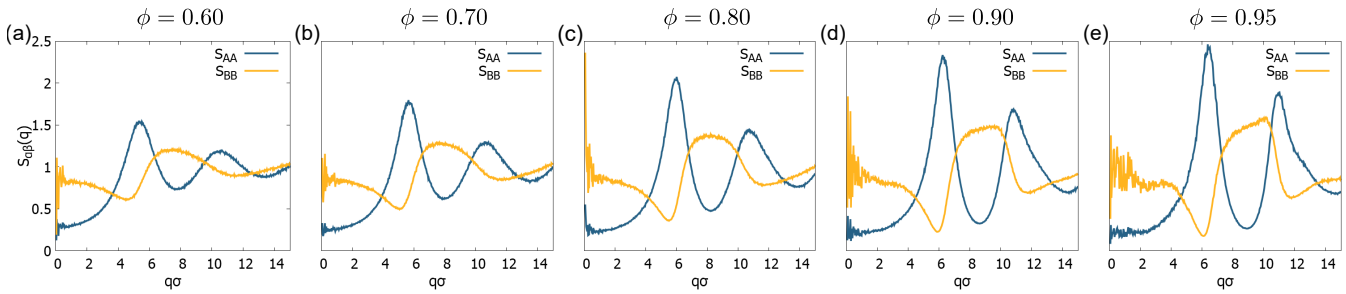

FIG. 7: Partial static structure factors $S_{\alpha\beta}(q)$ for the two different types of particles at different packing fractions. The blue color represent the largest particles ($\sigma_A = 1.2$) and the yellow color represents the smallest particles ($\sigma_B = 0.8$).

D. Structural relaxation time τ_α

The structural relaxation time can be computed by fitting our data with a stretched exponential function [8]:

$$f(t) = A \exp\left(-\left(\frac{B}{\tau_\alpha}\right)^{\alpha}\right), \tag{12}$$

where A, B and α are fitting parameters. Similarly, we can estimate τ_α by imposing that $F_c(q^*, \tau_\alpha) = 1/e$ represented in Fig. 2(d) and Fig. 4(c). Table I reports the different structural relaxation times.

TABLE I: Structural relaxation time τ_α as a function of the packing fraction ϕ (on the left), and as a function of the population that shifts their elasticity n_A (on the right).

ϕ	$\tau_\alpha[\tau]$
0.60	1.74
0.70	2.84
0.80	5.71
0.90	32.77
0.95	177.33

n_A [%]	$\tau_\alpha[\tau]$
10	42.16
20	27.82
25	18.96
50	8.38
100	3.94